

Trajectory and Power Design for Aerial CRNs with Colluding Eavesdroppers

Hongjiang Lei, Jiacheng Jiang, Haosi Yang, Ki-Hong Park,
Imran Shafique Ansari, Gaofeng Pan, and Mohamed-Slim Alouini

Abstract—Unmanned aerial vehicles (UAVs) can provide wireless access services to terrestrial users without geographical limitations and will become an essential part of the future communication system. However, the openness of wireless channels and the mobility of UAVs make the security of UAV-based communication systems particularly challenging. This work investigates the security of aerial cognitive radio networks (CRNs) with multiple uncertainties colluding eavesdroppers. A cognitive aerial base station transmits messages to cognitive terrestrial users using the spectrum resource of the primary users. All secondary terrestrial users and illegitimate receivers jointly decode the received message. The average secrecy rate of the aerial CRNs is maximized by jointly optimizing the UAV's trajectory and transmission power. An iterative algorithm based on block coordinate descent and successive convex approximation is proposed to solve the non-convex mixed-variable optimization problem. Numerical results verify the effectiveness of our proposed algorithm and show that our scheme improves the secrecy performance of airborne CRNs.

Index Terms—Unmanned aerial vehicle, trajectory and power design, average secrecy rate, multiple colluding eavesdroppers.

I. INTRODUCTION

A. Background and Related Works

Due to their high mobility, low cost, and on-demand deployment flexibility, unmanned aerial vehicles (UAVs) are considered critical to the future of the Internet of Things (IoT), enabling the interconnection of all things [1], [2]. More and more communication scenarios are now becoming flexible and diverse due to the inclusion of UAVs, such as UAV-assisted real-time surveillance, traffic control, and emergency disaster relief. In these application scenarios, UAV-assisted communication is considered to be an essential component of future mobile communication systems. By designing the

position of UAVs or optimizing their flight trajectory, the air-to-ground (A2G) links between UAVs and terrestrial nodes are line-of-sight (LoS) with a high probability. Therefore, the trajectory of UAVs has a decisive impact on the performance of the UAV-based communication system and becomes a fundamental problem to be solved in the design of airborne communication systems [3].

The concept of the “Internet of Everything” has led to an increasingly prominent role for UAVs in wireless communication systems [4]. UAV-assisted communication systems utilize drones to provide ubiquitous wireless coverage for a given area. In varying application scenarios, drones can be used in different roles in communication systems, such as base stations (BSs) [5] - [8], relays [9] - [11], and users [12] - [14]. In [5], a communication system consisting of multiple aerial BS was studied. The UAV trajectory was optimized to maximize the minimum throughput under the consideration of user scheduling coefficient and UAV transmit power. An efficient iterative algorithm based on successive convex approximation (SCA) and block coordinate descent (BCD) was proposed for mixed integer non-convex optimization. Their results showed that the proposed algorithm could improve the system's utility. Considering the limited energy consumption of UAVs' flight and ensuring the system's service quality, the author in [6] investigated the max-min fairness problem to maximize the throughput of the system by jointly optimizing the UAV transmit power and flight trajectory. In [7], a space-air-ground three-tier heterogeneous network consisted of a satellite, multiple UAVs, and multiple terrestrial BS to provide seamless coverage service for the ground users. A two-stage joint optimization was proposed to deal with the intra- and inter-interference and cross-tier resource allocation among different networks. A multi-UAVs-aided mobile edge computing system was designed to balance traffic and a new multi-UAV deployment mechanism was proposed in [8]. A near-optimal solution algorithm was proposed to solve the load-balancing multi-UAV deployment problem. When UAVs are used as relay nodes, long-distance wireless links between terrestrial BSs and terrestrial nodes (TNs) can be quickly established, which is helpful in disaster or other emergency scenarios [1]. In [9], authors considered a UAV-assisted cooperative system in which multiple UAVs were utilized as decode-and-forward relays to forward signals to the TNs. The minimum transmission rate of the system was maximized by jointly optimizing the flight trajectory of the relay UAVs, the transmit power on UAVs and terrestrial BS. An iterative algorithm was proposed to solve the joint optimization problem based on the block

Manuscript received.

This work was supported by the National Natural Science Foundation of China under Grant 61971080.

H. Lei is with the School of Communications and Information Engineering, Chongqing University of Posts and Telecommunications, Chongqing 400065, China and also is Chongqing Key Lab of Mobile Communications Technology, Chongqing 400065, China (e-mail: leihj@cqupt.edu.cn).

J. Jiang, and H. Yang are with the School of Communications and Information Engineering, Chongqing University of Posts and Telecommunications, Chongqing 400065, China (e-mail: cquptjic@163.com, cquptyhs@163.com).

I. S. Ansari Bharath Institute of Science and Technology, Chennai 600073, India (e-mail: ansarimran@ieee.org).

G. Pan is with the School of Cyberspace Science and Technology, Beijing Institute of Technology, Beijing 100081, China (e-mail: gaofeng.pan.cn@ieee.org).

K.-H. Park and M.-S. Alouini are with CEMSE Division, King Abdullah University of Science and Technology (KAUST), Thuwal 23955-6900, Saudi Arabia (e-mail: kihong.park@kaust.edu.sa, slim.alouini@kaust.edu.sa).

coordinate ascent technique, introducing the slack variable and SCA techniques. In [10], an aerial relay balanced the difference in transmission rates between free-space optical and radio frequency links. The throughput for delay-limited and delay-tolerant scenarios was maximized by carefully designing the flight trajectory of the aerial relay, which in turn maximized the throughput. Combining intelligent reflecting surface (IRS) and UAV can establish new channels or improve the A2G quality through full-angle reflection in the air. A UAV-IRS-aided covert scheme was proposed in [11], where the UAV carried an IRS and was utilized as a relay. Considering Willie's imperfect position state information, the covert transmission rate was maximized by alternately optimizing Alice's transmit power, IRS phase shift, and the horizontal position of the UAV-IRS. In UAV-aided wireless sensor networks and IoT communication systems, UAVs are utilized as aerial access points to disseminate/collect information to/from TNs [1]. A mixed-integer non-convex optimization problem was proposed to prolong the wireless sensor network lifetime and the UAV's trajectory was jointly optimized to minimize the maximum energy consumption of all sensor nodes in [12]. Refs. [13], [14] combined UAV trajectory design and wireless charging technology in the scenarios of the Internet of Things, considered the two-way link between information transmission and energy acquisition, and realized the problem of maximum and minimum data acquisition by optimizing the user scheduling coefficient and UAV flight trajectory.

The security of UAV communication applications is vulnerable to threats due to the broadcast nature and the prevailing LoS channel conditions [15], [16], [17]. Since then, more and more researches have focused on the security of UAV-based communication systems. The security of A2G and ground-to-air (G2A) links was investigated in [18], and the average secrecy rate (ASR) were maximized by jointly optimizing the transmission power and the trajectory of the UAV. By using successive convex approximation (SCA) and block coordinate descent (BCD), iterative algorithms were proposed to solve the non-convex problems. In [19], the security of underlay cognitive radio networks (CRNs) was investigated. The ASR was maximized by designing an antenna jammer's trajectory and transmit power. However, the eavesdroppers were assumed to operate in half-duplex mode and their position was assumed to be perfectly known.

The full-duplex (FD) eavesdroppers pose more severe security threats to UAV-based communication systems because they can not only intercept confidential information from A2G links but also send jamming signals to degrade the reception quality of the legitimate link. In [20], authors analyzed the security risks caused by terrestrial FD eavesdroppers and propose an iterative algorithm to maximize the ASRs of the downlink and uplink transmissions by optimizing the UAV flight trajectory and transmission power. The proposed non-convex problem was decomposed into sub-problems in BCD scheme with suboptimal solutions obtained by the SCA. The position of the eavesdroppers at the base stations was also assumed to be perfectly known.

Estimating the exact location and channel state information in these scenarios is very challenging, especially for malicious

eavesdroppers with some deception equipment. In these scenarios, the bounded eavesdropper's location error model was utilized and the worst ASR (WASR) was considered. Ref. [21] investigated the security of an A2G communication system with multiple eavesdroppers, whose locations are assumed to be imperfect. Another UAV was utilized as a friendly jammer to enhance the security of the UAV-aided communication, Ref. [22] designed both the aerial BS and the aerial jammer's transmit power and trajectories to maximize the WASR. The WASR and the secrecy energy efficiency (SEE) of the considered system were maximized by jointly optimizing the trajectory and transmit power of the aerial base station, respectively. Considering the imperfect location of the eavesdroppers and the practical propulsion energy consumption, two cooperative dual UAV-assisted data collection schemes have been proposed in [23]. The WASR and energy efficiency were maximized by optimizing the flight trajectory of the dual UAVs, the transmission power, and the scheduling coefficients. Furthermore, in some practical scenarios, multiple eavesdroppers attempt to intercept confidential information. In these scenarios, the base station needs to move away from all the eavesdroppers as far as possible and reach the legitimate targets as closely as possible to increase the secrecy rate. Authors in [24] studied the secrecy performance of the energy-constrained dual-UAV systems with multiple inaccurate location eavesdroppers. The WASR was maximized by optimizing the 3D trajectories, the transmit power of the airborne transmitter and jammer, and the time slot allocation scheme of the airborne transmitter. The security of an underlay CRN with multiple imprecise location eavesdroppers was investigated in [25]. The ASR of the cognitive user was maximized by optimizing the UAV's trajectory and transmission power. Authors in [26] investigated the secure CRNs and a friendly jammer was utilized to transmit artificial noise. Both scenarios were considered in which all the terrestrial nodes' locations were known and unknown. A dual collaborative underlay aerial IoT system with multiple uncertainty potential eavesdropper was considered and the WASR was maximized by jointly considering UAV trajectories, user scheduling, and transmit power in [28].

To maximize the eavesdropped information in some scenarios, the eavesdroppers may engage in colluding behavior, i.e., gathering and sharing information, especially in those scenarios where the quality of the eavesdropping links is poor. The most hazardous scenario is when all eavesdroppers are involved in malicious collusion [27]. The security of cellular UAV communication systems with multiple legitimate and illegitimate ground receivers was investigated in [29]. The secrecy rate of the UAV communication systems was maximized for both non-colluding and colluding scenarios by jointly optimizing the UAVs' 3D location and transmit power. However, the location of all eavesdroppers was assumed to be perfectly known. Authors in [30] studied the energy efficiency of a UAV-aided system with multiple colluding eavesdroppers with imperfect location information and formulated a mixed-integer non-convex optimization problem to minimize the energy consumption by jointly optimizing the UAV's trajectory and user scheduling. Authors in [31] investigated the secrecy performance of a UAV-aided non-orthogonal multiple access

TABLE I: *Related to Trajectory Design of UAV Communication Systems.*

Reference	Security	Role of UAVs	Imperfect Location of Eavesdroppers	Colluding Eavesdroppers	FD Eavesdroppers	CRNs
[5],[6]		BS				
[9]-[11]		Relay				
[12]-[14]		User				
[18]	✓	BS, User				
[19]	✓	Jammer				✓
[20]	✓	BS, User			✓	
[21]	✓	BS	✓			
[22]	✓	BS, Jammer	✓			
[23]	✓	User, Jammer	✓			
[24]	✓	BS, Jammer	✓			
[25]	✓	BS	✓			✓
[26]	✓	Jammer	✓			✓
[27]	✓	BS		✓		
[28]	✓	BS, Jammer	✓			✓
[29]	✓	BS		✓	✓	
[30]	✓	BS	✓	✓		
[31]	✓	BS	✓	✓		
Our Work	✓	BS	✓	✓	✓	✓

(NOMA) systems with multiple colluding eavesdroppers with imperfect location information. The minimum WASR was maximized by jointly optimizing the UAV's trajectory, the transmit power, and the power allocation coefficient. Table I outlines recent works in literature related to trajectory design of UAV communication systems.

B. Motivation and Contributions

The previous discussed works demonstrated that the security of UAV-aided CRNs can be significantly improved by designing the UAV's trajectory and other system parameters (such as transmit power). However, these outstanding works did not answer the following security issue: *How to design the trajectory and transmit power of the aerial base station where multiple inaccurate location FD eavesdroppers intercept information in colluding mode? What is the optimal secrecy performance of the aerial CRNs with multiple colluded FD eavesdroppers with imperfect location?* Hence, this work answers these questions by optimizing the WASR of aerial CRNs. It is assumed that multiple location-uncertainty illegitimate receivers work in FD and colluding modes and the legitimate receivers jointly decode the received legitimate messages via maximal ratio combining (MRC) scheme. The main contributions of this work are summarized as follows:

- 1) We consider an underlay CRN consisting of an aerial base station and multiple primary and cognitive users. Multiple malicious FD eavesdroppers at uncertain locations wiretap confidential information and transmit interference to degrade the reception quality of the legitimate links. All terrestrial secondary users and illegitimate receivers are assumed to utilize the cooperative decoding of received message, respectively. The WASR is maximized by jointly optimizing the UAV's transmission power and trajectory while satisfying SEE limit. Due to its non-convexity, the optimization problem is split into two sub-problems and transformed into approximated convex forms via SCA. The BCD technique is utilized to solve these subproblems.

- 2) The proposed algorithm's convergence and complexity are analyzed and the numerical results of the proposed scheme are compared with three benchmarks where the aerial base station works with the fixed trajectory and transmits power simultaneously or only optimizing the trajectory and transmit power separately. The efficiency and the convergence of the proposed algorithm are verified.
- 3) Relative to [19], [25], [26], [28] where the secure CRNs with a single eavesdropper was considered, this work investigates the security of aerial CRNs with multiple colluding eavesdroppers residing at uncertain location. Technically speaking, considering the collusion scenarios is much more challenging than the independent eavesdropping scenarios.
- 4) Although the colluding scenarios were considered in [27] and [29], the results can not be applied to CRNs directly since the location of the eavesdroppers is assumed to be perfectly known and the underlay condition was not considered. This work assumes that both legitimate and illegitimate receivers are considered jointly to decode the received legitimate messages. Both the uncertainty of eavesdroppers' locations and the underlay condition are considered simultaneously.

C. Organization

The rest of this paper is organized as follows. The system model and problem formulation are provided in Section II and III, respectively. A two-step alternating algorithm is proposed in Section IV to solve the problem. Simulation results are demonstrated in Section V. Finally, Section VI concludes this paper. TABLE II lists the notations and symbols utilized in this work.

II. SYSTEM MODEL

As shown in Fig. 1, we consider an aerial underlay communication system consisting of a rotary-wing UAV that works as a base station (S) and multiple terrestrial users

TABLE II: List of Notations.

Notation	Description
\mathbf{q}_S^0	Initial location of S
\mathbf{q}_S^f	Final location of S
\mathbf{w}_{D_k}	Horizontal location of D_k
$\mathbf{w}_{E_m}, \hat{\mathbf{w}}_{E_m}$	Exact and estimated location of E_m
\mathbf{w}_{U_r}	Horizontal location of U_r
r_{E_m}	Maximized estimation errors of the distance
H	Altitude of S
Γ_r	Tolerance threshold of U_r
σ^2	The noise power
P_S^{\max}	The peak transmit power of S
P_E	Transmit power of E_m
α	Path loss exponent
V_S^{\max}	Maximum flight speed of the UAV
β_0	Channel power gain at the reference distance
δ_t	Time slot length
ε	Algorithm convergence precision
Ψ	SEE threshold of S

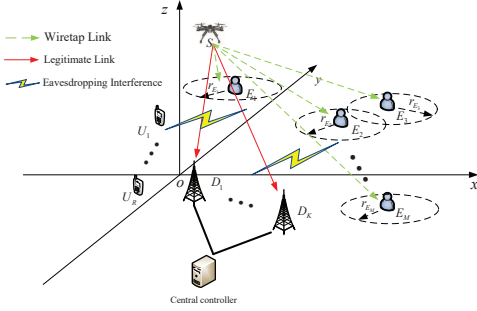


Fig. 1: UAV-enabled CRN consists of an aerial base station (S), multiple primary users (U_r), and multiple cognitive users (D_k). Multiple FD eavesdroppers (E_m) at uncertain locations not only try to wiretap the confidential information but also send interference to degenerate the reception quality of the legitimate link.

($D_k, k = 1, \dots, K$) in the presence of multiple primary users ($U_r, r = 1, \dots, R$) and multiple malicious FD eavesdroppers ($E_m, m = 1, \dots, M$). All the nodes are equipped with a single antenna.

To avoid collisions, S flies at a constant altitude H that is higher than the highest obstacle in the service area [21], [23], [25], [32]. The flight period, T , is divided into N time slots as $\delta_t = \frac{T}{N}$ [3]. Without loss of generality, a 3D cartesian coordinate is used. Then the coordinates of S , D_k , U_r , and E_m are written as $\mathbf{q}_S(n) = [x_S(n), y_S(n)]^T$, $\mathbf{w}_{D_k} = [x_{D_k}, y_{D_k}]^T$, $\mathbf{w}_{U_r} = [x_{U_r}, y_{U_r}]^T$, and $\mathbf{w}_{E_m} = [x_{E_m}, y_{E_m}]^T$, respectively, where $n = 1, \dots, N$.

Similar to [19] and [23], the A2G links are assumed to be LoS links and the channel coefficient between S and the terrestrial receiver i is expressed as

$$h_{S_i}(n) = \frac{\beta_0}{d_{S_i}^2(n) + H^2}, \quad (1)$$

where $i \in \{D_k, U_r, E_m\}$, β_0 denotes the channel power gain at the reference distance and $d_{S_i}(n) = \|\mathbf{q}_S(n) - \mathbf{w}_i\|$ signifies the Euclidean distance between S and i , respectively.

Due to the uncertainty of the eavesdroppers' locations, h_{SE} obtained by (1) is imperfect. We define $\hat{\mathbf{w}}_{E_m} \in \mathbb{R}^{2 \times 1}$ and r_{E_m} to express the estimated location and maximum error of the difference between the estimation and the practical distance, respectively. According to [23], it is assumed that $\|\mathbf{q}_S(n) - \hat{\mathbf{w}}_{E_m}\| \geq r_{E_m}$. Following the triangle inequality, d_{SE_m} is expressed as

$$\begin{aligned} d_{SE_m}(n) &= \|\mathbf{q}_S(n) - \mathbf{w}_{E_m}\| \\ &\geq \|\|\mathbf{q}_S(n) - \hat{\mathbf{w}}_{E_m}\| - \|\hat{\mathbf{w}}_{E_m} - \mathbf{w}_{E_m}\|\| \\ &\geq \left| \underbrace{\|\mathbf{q}_S(n) - \hat{\mathbf{w}}_{E_m}\|}_{\triangleq \hat{d}_{SE_m}(n)} - r_{E_m} \right|, \end{aligned} \quad (2)$$

where $\hat{d}_{SE_m}(n)$ denotes the estimation of $d_{SE_m}(n)$.

The ground-to-ground (G2G) link between D_k and E_m is assumed to undergo quasi-static Rayleigh model, then channel coefficient is expressed as

$$h_{D_k E_m} = \frac{\beta_0}{d_{D_k E_m}^\alpha} \xi_{D_k E_m}, \quad (3)$$

where $d_{D_k E_m} = \|\mathbf{w}_{D_k} - \mathbf{w}_{E_m}\|$ signifies the Euclidean distance between D_k and E_m , $\xi_{D_k E_m}$ follows an exponential distribution with unit mean, and $\alpha > 2$ denotes the path-loss exponent. Similarly, the distance between D_k and E_m is expressed as

$$\begin{aligned} d_{D_k E_m} &= \|\mathbf{w}_{D_k} - \mathbf{w}_{E_m}\| \\ &\geq \|\|\mathbf{w}_{D_k} - \hat{\mathbf{w}}_{E_m}\| - \|\hat{\mathbf{w}}_{E_m} - \mathbf{w}_{E_m}\|\| \\ &\geq \left| \underbrace{\|\mathbf{w}_{D_k} - \hat{\mathbf{w}}_{E_m}\|}_{\triangleq \hat{d}_{D_k E_m}} - r_{E_m} \right|. \end{aligned} \quad (4)$$

where $\hat{d}_{D_k E_m}$ signifies the estimation of $d_{D_k E_m}$. Then h_{SE_m} and $h_{D_k E_m}$ are approximated by

$$\hat{h}_{SE_m}(n) = \frac{\beta_0}{\left(\hat{d}_{SE_m}(n) - r_{E_m}\right)^2 + H^2}, \quad (5)$$

and

$$\hat{h}_{D_k E_m} = \frac{\beta_0}{A_{k,m}^\alpha} \xi_{D_k E_m}, \quad (6)$$

respectively, where $A_{k,m} = \left|\hat{d}_{D_k E_m} - r_{E_m}\right|$.

Due to the presence of FD eavesdropper nodes, the signal-to-interference-plus-noise ratio (SINR) at D_k is expressed as

$$\gamma_{D_k}(n) = \frac{P_S(n) h_{SD_k}(n)}{\sum_{i=1}^M P_{E_m}(n) \hat{h}_{D_k E_m} + \sigma^2}, \quad (7)$$

where $P_S(n)$ and $P_{E_m}(n)$ denote the transmit power of the S and E_m , respectively, and σ^2 signifies the variance of additive white Gaussian noise (AWGN).

With the coordinated multi-point (CoMP) reception, all the cognitive users jointly decode the received legitimate messages

via maximal ratio combining (MRC) scheme [29]. Then the achievable rate at the legitimate receiver is expressed as

$$\begin{aligned} R_S(n) &\approx \mathbb{E}_\xi \left[\log_2 \left(1 + \sum_{k=1}^K \gamma_{D_k}(n) \right) \right] \\ &= \mathbb{E}_\xi \left[\log_2 \left(1 + \sum_{k=1}^K \frac{P_S(n) h_{SD_k}(n)}{\sum_{m=1}^M P_{E_m}(n) \hat{h}_{D_k E_m} + \sigma^2} \right) \right], \end{aligned} \quad (8)$$

where $\mathbb{E}[\cdot]$ denotes the expectation.

Since $\hat{h}_{D_k E_m}(n)$ in (6) is convex with respect to ξ , $R_S(n)$ in (8) is convex with respect to $\hat{h}_{D_k E_m}(n)$, based on Jensen's inequality, we approximate the achievable at the legitimate receiver as [33]

$$\begin{aligned} R_S(n) &\geq \log_2 \left(1 + \sum_{k=1}^K \frac{P_S(n) h_{SD_k}(n)}{\sum_{m=1}^M P_{E_m}(n) \mathbb{E}_\xi [\hat{h}_{D_k E_m}] + \sigma^2} \right) \\ &= \log_2 \left(1 + \sum_{k=1}^K \frac{P_S(n) h_{SD_k}(n)}{\beta_0 \sum_{m=1}^M P_{E_m}(n) A_{k,m}^{-\alpha} + \sigma^2} \right) \\ &\triangleq R_S^L(n), \end{aligned} \quad (9)$$

where the superscript 'L' signifies the lower bound.

Similarly to (7), the SINR at the m th E can also be expressed as

$$\gamma_{SE_m}(n) = \frac{P_S(n) \hat{h}_{SE_m}(n)}{\sum_{j \neq m} P_{E_j}(n) \hat{h}_{E_j E_m} + \sigma^2}, \quad (10)$$

where $h_{E_j E_m}$ denotes the interference from other eavesdroppers.

It is assumed that all the eavesdroppers transmit signals with its maximum power over the whole period and cooperatively intercept/decode the confidential message from S . Thus, we have $P_{E_m}(n) = P_E$. Moreover, the worst-case scenario is considered, the interference from other eavesdroppers is assumed to be perfectly cancelled [20]. Therefore, we obtain the SINR at the illegitimate receiver as

$$\begin{aligned} R_E(n) &= \log_2 \left(1 + \sum_{m=1}^M \gamma_{SE_m}(n) \right) \\ &= \log_2 \left(1 + \sum_{m=1}^M \frac{P_S(n) \hat{h}_{SE_m}(n)}{P_E \sum_{j \neq m} h_{E_j E_m} + \sigma^2} \right) \\ &= \log_2 \left(1 + \sum_{m=1}^M \frac{P_S(n) \hat{h}_{SE_m}(n)}{\sigma^2} \right). \end{aligned} \quad (11)$$

Then the achievable secrecy rate of the considered system is

approximated as

$$\begin{aligned} R_{\text{sec}}(n) &= [\log_2 (R_S^L(n) - R_E(n))]^+ \\ &= \left[\log_2 \left(\frac{1 + \sum_{k=1}^K \frac{P_S(n) h_{SD_k}(n)}{\beta_0 P_E \sum_{m=1}^M A_{k,m}^{-\alpha} + \sigma^2}}{1 + \sum_{m=1}^M \frac{P_S(n) \hat{h}_{SE_m}(n)}{\sigma^2}} \right) \right]^+, \end{aligned} \quad (12)$$

where $[x]^+ = \max\{0, x\}$. Then the SEE of the considered system is expressed as [23]

$$\mu = \frac{\sum_{n=1}^N R_{\text{sec}}(n)}{\sum_{n=1}^N P_S(n)}. \quad (13)$$

At the n time slot, the interference at U_r is expressed as

$$\begin{aligned} \hat{I}_r(n) &= P_S(n) h_{SU_r}(n) + P_E \sum_{m=1}^M \mathbb{E}_\xi [h_{E_m U_r}] \\ &\stackrel{(a)}{\leq} P_S(n) h_{SU_r}(n) + P_E \sum_{m=1}^M \frac{\beta_0}{d_{E_m U_r}^\alpha} \\ &\triangleq I_r(n), \end{aligned} \quad (14)$$

where $h_{E_m U_r} = \frac{\beta_0}{d_{E_m U_r}^\alpha} \xi_{E_m U_r}$ denotes the channel coefficient between E_m and U_r , $\xi_{E_m U_r}$ follows an exponential distribution with unit mean, step (a) is obtained based on Jensen's inequality [34] and $d_{E_m U_r} = \|\mathbf{w}_{U_r}(n) - \hat{\mathbf{w}}_{E_m}\| - r_{E_m}$. To ensure the quality of service (QoS) of the primary users, the average interference caused by S and E_m must be limited to the interference temperature (IT) threshold, Γ_r , [19], [25], and [26]. Thus, we have

$$\frac{1}{N} \sum_{n=1}^N I_r(n) \leq \Gamma_r, \forall r. \quad (15)$$

III. PROBLEM FORMULATION

This work optimizes the WASR of the aerial CRNs by designing S 's horizontal trajectory and transmission power, while the SEE is guaranteed. Let $\mathbf{Q} = \{\mathbf{q}_S(n), \forall n\}$, $\mathbf{P} = \{P_S(n), \forall n\}$. Thus, the optimization problem is formulated as

$$\mathcal{P}_1 : \max_{\mathbf{P}, \mathbf{Q}} \frac{1}{N} \sum_{n=1}^N R_{\text{sec}}^1(n) \quad (16a)$$

$$\text{s.t. } \mu \geq \Psi, \quad (16b)$$

$$0 \leq P_S(n) \leq P_S^{\max}, \forall n, \quad (16c)$$

$$\frac{1}{N} \sum_{n=1}^N I_r(n) \leq \Gamma_r, \forall r, \quad (16d)$$

$$\mathbf{q}_S(0) = \mathbf{q}_S^I, \mathbf{q}_S(n) = \mathbf{q}_S^F, \quad (16e)$$

$$\|\mathbf{q}_S(n) - \mathbf{q}_S(n-1)\| \leq V_S^{\max} \delta_t, \forall n, \quad (16f)$$

where Ψ is the SEE threshold, P_S^{\max} is the peak transmit power of S , \mathbf{q}_S^I and \mathbf{q}_S^F signify the initial and final position of S , respectively, V_S^{\max} denotes the maximum speed of S , (16b)

is the SEE constraint, (16c) is the power constraint, (16d) is the constraint to ensure that the primary users work properly, (16e) is the constraint for the initial and final position of UAVs, and (16f) is the constraint for the maximum flight path in adjacent periods of flight.

\mathcal{P}_1 is challengeable to solve since the operator $[x]^+$ makes the objective function non-smooth at zero value. Moreover, \mathcal{P}_1 is a multivariate coupled optimization problem, which is non-convex concerning horizontal trajectory variables \mathbf{Q} and the transmit power variables \mathbf{P} .

IV. PROPOSED ALGORITHM FOR PROBLEM \mathcal{P}_1

To deal with the non-smoothness of $R_{\text{sec}}(n)$, according to Lemma 1 in [18] and [19], removing the operator $[x]^+$ does not affect the optimal value of \mathcal{P}_1 because the secrecy rate can be obtained by setting the transmit power to zero when it is less than zero. Simultaneously, based on the alternating optimization (AO) method, \mathbf{Q} and \mathbf{P} are optimized in an alternating manner, taking into account the other given variables.

A. Subproblem 1: Optimization Transmit Power of S

In this subsection, we optimize \mathbf{P} , the transmit power of S , with given \mathbf{Q} . The original problem \mathcal{P}_1 is rewritten as

$$\mathcal{P}_{1.1} : \max_{\mathbf{P}} \frac{1}{N} \sum_{n=1}^N R_{\text{sec}}^1(n) \quad (17a)$$

$$\text{s.t. } \mu_1 \geq \Psi, \quad (17b)$$

$$(16c), (16d), \quad (17c)$$

where $\mu_1 = \frac{\sum_{n=1}^N R_{\text{sec}}^1(n)}{\sum_{n=1}^N P_S(n)}$, $R_{\text{sec}}^1(n) = \log_2(1 + A_n P_S(n)) - \log_2(1 + B_n P_S(n))$, $A_n = \sum_{k=1}^K \frac{h_{SD_k}(n)}{\beta_0 P_E \sum_{m=1}^M A_{k,m}^{-\alpha} + \sigma^2}$, and $B_n = \sum_{i=1}^M \frac{\hat{h}_{SE_m}(n)}{\sigma^2}$.

To tackle the non-convex characterization in (17a) and (17b), the first-order Taylor expansion is utilized to approximate $R_{\text{sec}}^1(n)$ as

$$R_{\text{sec}}^2(n) = \log_2(1 + A_n P_S(n)) - \log_2(1 + B_n P_S^{(l)}(n)) - \frac{B_n}{\ln(2)(1 + B_n P_S^{(l)}(n))} (P_S(n) - P_S^{(l)}(n)), \quad (18)$$

where $P_S^{(l)}(n)$ is a given feasible point in the l th iteration. Then $\mathcal{P}_{1.1}$ is approximated as

$$\mathcal{P}_{1.2} : \max_{\mathbf{P}} \frac{1}{N} \sum_{n=1}^N R_{\text{sec}}^2(n) \quad (19a)$$

$$\text{s.t. } \sum_{n=1}^N R_{\text{sec}}^2(n) \geq \Psi \sum_{n=1}^N P_S(n), \quad (19b)$$

$$(16c), (16d). \quad (19c)$$

$\mathcal{P}_{1.2}$ is a convex problem and can be solved by existing optimization tools such as CVX.

B. Subproblem 2: Optimizing Trajectory of S

Given \mathbf{P} , \mathcal{P}_1 is rewritten as

$$\mathcal{P}_{2.1} : \max_{\mathbf{Q}} \frac{1}{N} \sum_{n=1}^N R_{\text{sec}}^3(n) \quad (20a)$$

$$\text{s.t. } \mu_2 \geq \Psi, \quad (20b)$$

$$\frac{1}{N} \sum_{n=1}^N I_r^{\mathbf{Q}}(n) \leq \Gamma_r, \forall r, \quad (20c)$$

$$(16e), (16f), \quad (20d)$$

where $\mu_2 = \frac{\sum_{n=1}^N R_{\text{sec}}^3(n)}{\sum_{n=1}^N P_S(n)}$, $R_{\text{sec}}^3(n) = \log_2 \left(1 + \sum_{k=1}^K \frac{f_{1,k}}{d_{SD_k}^2 + H^2} \right) - \log_2 \left(1 + \sum_{m=1}^M \frac{f_2}{(\hat{d}_{SE_m} - r_{E_m})^2 + H^2} \right)$, $f_{1,k} = \frac{P_S(n)}{P_E \sum_{m=1}^M A_{k,m}^{-\alpha} + \frac{1}{\rho_0}}$, $f_2 = \rho_0 P_S(n)$, $I_r^{\mathbf{Q}}(n) = \frac{P_S(n) \rho_0}{d_{SU_r}^2 + H^2} + P_E \sum_{m=1}^M h_{E_m U_r}$, and $\rho_0 = \frac{\beta_0}{\sigma^2}$.

It must be noted that $\mathcal{P}_{2.1}$ is a non-convex problem because the objective function in (20a) is a non-concave function with respect to $\mathbf{q}_S(n)$ and (20b) and (20c) are non-convex constraints with respect to $\mathbf{q}_S(n)$.

By introducing new slack variables and using the successive convex approximation (SCA), we obtain

$$R_{\text{sec}}^3(n) \geq \log_2 \left(1 + \sum_{k=1}^K \frac{f_{1,k}}{\tilde{\zeta}_k^{(l)}(n)} \right) - \log_2 \left(1 + \sum_{m=1}^M \frac{f_2}{\tilde{\xi}_m^{(l)}(n)} \right) - \frac{\sum_{k=1}^K \left(\frac{f_{1,k}}{(\tilde{\zeta}_k^{(l)}(n))^2} (\tilde{\zeta}_k(n) - \tilde{\zeta}_k^{(l)}(n)) \right)}{\ln(2) \left(1 + \sum_{k=1}^K \frac{f_{1,k}}{\tilde{\zeta}_k^{(l)}(n)} \right)} \triangleq R_{\text{sec}}^{3,\mathbf{L}}(n), \quad (21)$$

where the superscript ' l ' denotes the iteration index, $\tilde{\zeta}_k(n)$ and $\tilde{\xi}_m(n)$ are new slack variables, which must satisfy

$$\tilde{\zeta}_k(n) \geq d_{SD_k}^2 + H^2 \quad (22)$$

and

$$\tilde{\xi}_m(n) \leq (\hat{d}_{SE_m} - r_{E_m})^2 + H^2, \quad (23)$$

respectively. Due to the right-hand-side of (23) is convex which makes (23) become non-convex. According to SCA, (23) is rewritten as

$$\tilde{\xi}_m(n) \leq H^2 - 2r_{E_m} \|\mathbf{q}_S(n) - \mathbf{w}_{E_m}\| + r_{E_m}^2 + 2(\mathbf{q}_S(n) - \mathbf{w}_{E_m})^T (\mathbf{q}_S(n) - \mathbf{q}_S^{(l)}(n)) + \|\mathbf{q}_S^{(l)}(n) - \mathbf{w}_{E_m}\|^2. \quad (24)$$

With the same method, (20c) is rewritten as

$$\frac{1}{N} \sum_{n=1}^N \left(\frac{\rho_0 P_S(n)}{\tilde{d}_{SU_r} + H^2} + P_E \sum_{m=1}^M h_{E_m U_r} \right) \leq \Gamma_r, \quad (25)$$

TABLE III: List of Simulation Parameters.

Parameter	Value
\mathbf{q}_S^0	$[-300, -200]^T, [-250, 800]^T$
\mathbf{q}_S^F	$[100, -200]^T, [0, -200]^T$
\mathbf{w}_{D_k}	$[-200, 500; -100, 500; 0, 500]^T$ $[-100, 300; -50, 400; 0, 300]^T$ $[-250, 300; -100, 0; 50, 300]^T$
$\hat{\mathbf{w}}_{E_m}$	$[-150, 700; -50, 700]^T$ $[-125, 100; -150, 200]^T$ $[-200, -20; 0, -20]^T$
\mathbf{w}_{U_r}	$[-100, 0]^T$ $[-200, 400]^T$ $[-100, 400]^T$
r_{E_m}	10 m, 30 m
H	100 m
Γ_r	-110 dBm
σ^2	-110 dBm
P_S^{\max}	3 W
P_E	0.1 W
α	2.2
V_S^{\max}	60 m/s
β_0	-60 dB
δ_t	1 s
ε	0.01
Ψ	1

where \tilde{d}_{SU_r} is a new slack variable which satisfies

$$\tilde{d}_{SU_r} \leq \left\| \mathbf{q}_S^{(l)}(n) - \mathbf{w}_r \right\|^2 + 2(\mathbf{q}_S(n) - \mathbf{w}_r)^T (\mathbf{q}_S(n) - \mathbf{q}_S^{(l)}(n)). \quad (26)$$

Based on the above conversion, $\mathcal{P}_{2.1}$ is approximated as

$$\mathcal{P}_{2.2} \max_{\mathbf{q}_S, \tilde{\xi}_m(n), \tilde{\zeta}_k(n), \tilde{d}_{SU_r}} \frac{1}{N} \sum_{n=1}^N R_{\text{sec}}^{3, \mathbf{L}}(n) \quad (27a)$$

$$\text{s.t. } \mu_3 \geq \Psi, \quad (27b)$$

$$\frac{1}{N} \sum_{n=1}^N \frac{\beta_0 P_S(n)}{\tilde{d}_{SU_r} + H^2} + P_E \sum_{m=1}^M h_{E_m U_r} \leq \Gamma_r, \forall r, \quad (27c)$$

$$\tilde{\zeta}_k(n) \geq d_{SD_k}^2 + H^2, \forall n, \forall k, \quad (27d)$$

$$\tilde{\xi}_m(n) \leq H^2 - 2r_{E_m} \|\mathbf{q}_S(n) - \mathbf{w}_{E_m}\| + r_{E_m}^2 + 2(\mathbf{q}_S(n) - \mathbf{w}_{E_m})^T (\mathbf{q}_S(n) - \mathbf{q}_S^{(l)}(n)) \quad (27e)$$

$$+ \left\| \mathbf{q}_S^{(l)}(n) - \mathbf{w}_{E_m} \right\|^2, \forall n, \forall m, \quad (27f)$$

$$\tilde{d}_{SU_r} \leq \left\| \mathbf{q}_S^{(l)}(n) - \mathbf{w}_r \right\|^2 + 2(\mathbf{q}_S(n) - \mathbf{w}_r)^T (\mathbf{q}_S(n) - \mathbf{q}_S^{(l)}(n)), \forall n, \forall r, \quad (27g)$$

$$(16e), (16f), \quad (27g)$$

where $\mu_3 = \frac{\sum_{n=1}^N R_{\text{sec}}^{3, \mathbf{L}}(n)}{\sum_{n=1}^N P_S(n)}$. Now $\mathcal{P}_{2.2}$ is convex and can be solved with existing optimisation tools.

C. Convergence Analysis of Algorithm 1

Combining the above two subproblems and applying BCD, an iterative algorithm for solving \mathcal{P}_1 is proposed. The sub-

Algorithm 1: Iterative Procedure of Problem \mathcal{P}_1

Input: Initialization of feasible points.
while $R_{\text{sec}}(\mathbf{P}^{(l+1)}, \mathbf{Q}^{(l+1)}) - R_{\text{sec}}(\mathbf{P}^{(l)}, \mathbf{Q}^{(l)}) \geq \varepsilon$ **do**
 1. Solve $(\mathcal{P}_{1.2})$ for given $\mathbf{Q}^{(l)}$ and obtain the solution $\mathbf{P}^{(l+1)}$;
 2. Solve $(\mathcal{P}_{2.2})$ for given $\mathbf{P}^{(l+1)}$ and obtain the solution $\mathbf{Q}^{(l+1)}$;
 3. $l = l + 1$;
 4. Calculate $R_{\text{sec}}(\mathbf{P}^{(l+1)}, \mathbf{Q}^{(l+1)})$.
end
Output: $R_{\text{sec}}(\mathbf{P}^{(l+1)}, \mathbf{Q}^{(l+1)})$ with $\mathbf{P}^* = \mathbf{P}^{(l+1)}, \mathbf{Q}^* = \mathbf{Q}^{(l+1)}$.

optimal solution is obtained by selecting the initial feasible points and solving $\mathcal{P}_{1.2}$ and $\mathcal{P}_{2.2}$ alternatively. Each iteration's solutions serve as feasible input values at the next iteration. The objective function of the original problem \mathcal{P}_1 at the l th iteration is defined as $R_{\text{sec}}(\mathbf{P}^l, \mathbf{Q}^l)$, meanwhile, the details of the entire iteration of \mathcal{P}_1 are summarized in Algorithm 1, where the tolerance of the convergence of the algorithm is denoted as ε . The convergence of Algorithm 1 is proved as follows.

Proof. In Step 1 of **Algorithm 1**, the power allocation of UAV solved by applying interior point method. Thus, we have

$$R_{\text{sec}}(\mathbf{P}^{(l)}, \mathbf{Q}^{(l)}) \leq R_{\text{sec}}^{\mathbf{L}, 1}(\mathbf{P}^{(l+1)}, \mathbf{Q}^{(l)}) \leq R_{\text{sec}}(\mathbf{P}^{(l+1)}, \mathbf{Q}^{(l)}), \quad (28)$$

where the objective function of problem $\mathcal{P}_{1.2}$ is lower-bounded by $R_{\text{sec}}^{\mathbf{L}, 1}(\mathbf{P}^{(l+1)}, \mathbf{Q}^{(l)})$. Then, by solving $\mathcal{P}_{2.2}$ the suboptimal solution $\mathbf{Q}^{(l+1)}$ is obtained, and have

$$R_{\text{sec}}(\mathbf{P}^{(l+1)}, \mathbf{Q}^l) \leq R_{\text{sec}}^{\mathbf{L}, 2}(\mathbf{P}^{(l+1)}, \mathbf{Q}^{(l+1)}) \leq R_{\text{sec}}(\mathbf{P}^{(l+1)}, \mathbf{Q}^{(l+1)}), \quad (29)$$

where the objective function of problem $\mathcal{P}_{2.2}$ is lower-bounded by $R_{\text{sec}}^{\mathbf{L}, 2}(\mathbf{P}^{(l+1)}, \mathbf{Q}^{(l+1)})$.

The objective function is always non-decreasing after each iteration, as shown in (29). Meanwhile, we additionally notice that due to the feasible set under the constraints, the objective function in \mathcal{P}_1 is upper bounded by a finite value. Therefore, Algorithm 1 is convergent. \square

The complexity of **Algorithm 1** comes from two aspects. One is optimizing transmit power of S , the other is solving S 's trajectory. They are solved by the interior point method with complexity $\mathcal{O}(\phi^{3.5} \ln(\frac{1}{\varsigma}))$ and $\mathcal{O}(\varphi^{3.5} \ln(\frac{1}{\varsigma}))$, respectively, where $\phi = 2N + R + 1$, $\varphi = NK + NM + NR + N + R + 5$, and ς denotes convergence precision. It is assumed that the number of iterations is I . Thus, the total complexity of **Algorithm 1** is $\mathcal{O}(I \ln(\frac{1}{\varsigma}) (\phi^{3.5} + \varphi^{3.5}))$.

V. NUMERICAL RESULTS AND ANALYSIS

In this section, simulation results are presented to verify the performance of the joint transmit power control and UAV

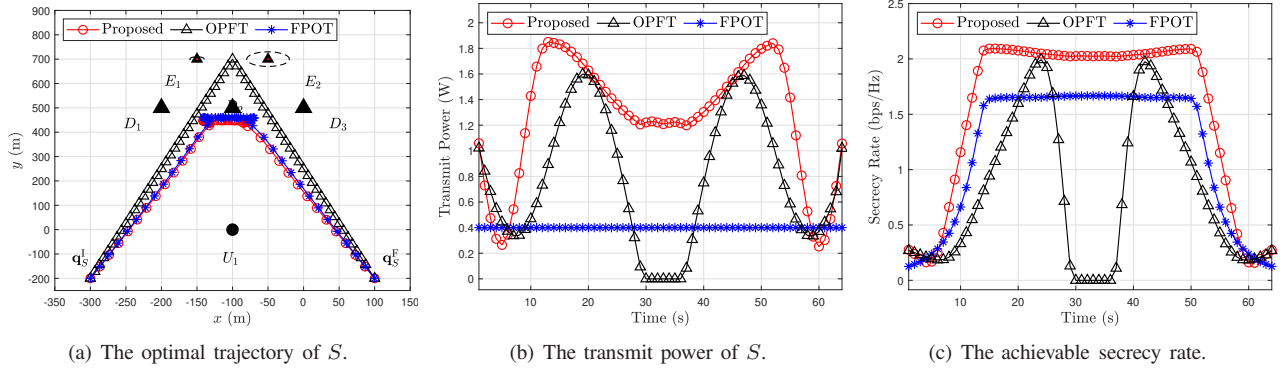


Fig. 2: Scenario 1 wherein the FD-eavesdroppers are uniformly distributed with $K = 3$ terrestrial users.

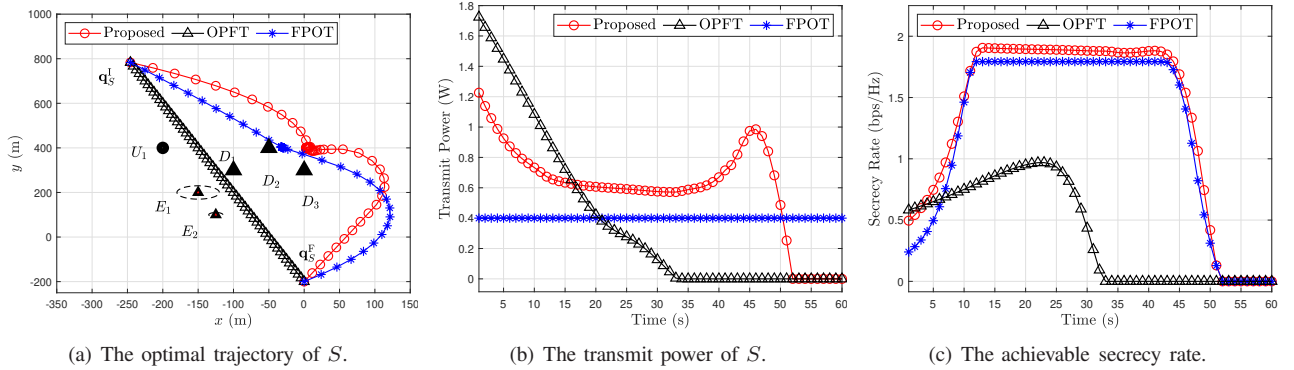


Fig. 3: Scenario 2 wherein the FD-eavesdroppers are cluster distributed with $K = 3$ terrestrial users.

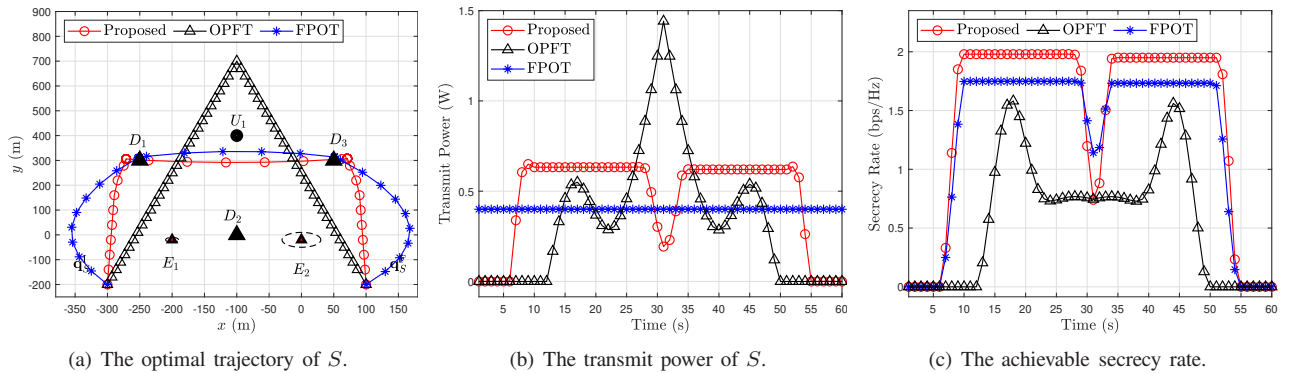


Fig. 4: Scenario 3 wherein the FD-eavesdroppers are interweaved in space with $K = 3$ terrestrial users.

trajectory optimization algorithm. To verify the effectiveness of our proposed algorithm, three scenarios are considered, in which the two FD-eavesdroppers are uniformly distributed, cluster distributed, and interweaved distributed with three terrestrial users, respectively. The details of parameter setup are listed in Table III. Similar to [18], [19], [20], the following benchmark schemes are also considered : 1) Benchmark 1: S operates with a fixed transmission power and a fixed trajectory, which is the initial value for the optimized transmit power and trajectory (denoted as FPFT). 2) Benchmark 2: S works with fixed transmit power and the trajectory is optimized (denoted as FPOT). 3) Benchmark 3: S works with fixed trajectory and its transmission power is optimized (denoted as OPFT).

To illustrate the effect of colluding FD eavesdroppers, the trajectory obtained with different schemes for the different scenarios is shown in Figs. 2 - 4. For the FPOT scheme where S works with fixed power, it should try to stay away from the area where the eavesdroppers are located while getting close to the legitimate users. For the OPFT scheme where S flies with a given trajectory, the transmit power should be reduced (to zero) as it approaches the area where the eavesdroppers are located to avoid the information being eavesdropped. In the proposed scheme, the power is gradually increased/decreased to maximize the secrecy rate as it approaches the legitimate users (such as D_1 in Figs. 2(a) and 4(a)) and ensure that the interference to the primary user does not exceed the IT thresh-

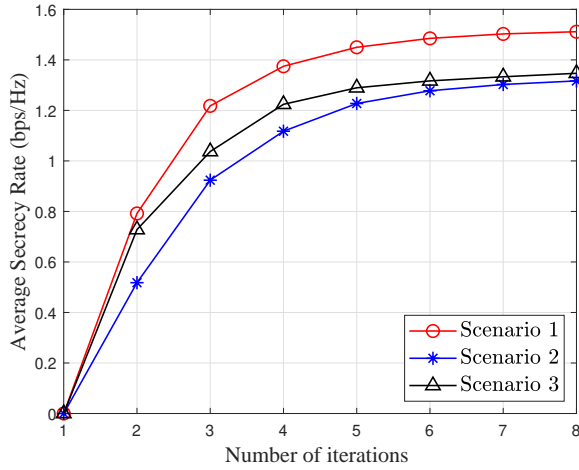


Fig. 5: The WASR versus the number of iterations for different scenarios.

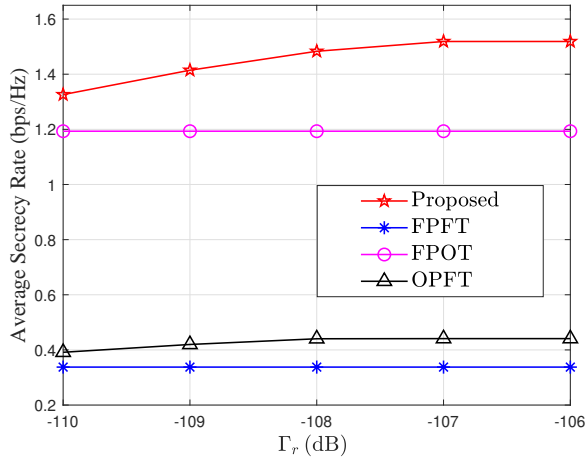


Fig. 6: The WASR versus Γ_r with different schemes.

old. As S flies, it gradually moves away from the legitimate users and approaches the area where the eavesdroppers are located, and the transmission power is reduced to avoid the information being wiretapped. The characteristics of FPOT and OPFT are considered simultaneously to obtain the optimal secrecy performance. It can be observed from Fig. 4(c) that the achievable secrecy rate of FPOT is higher than that of the proposed at 31s. This is because the optimized transmit power of the proposed is lower to decrease the interference to the primary user. We note that the optimality of the proposed scheme does not mean the proposed scheme is time-pieceswise optimal but time-averaged optimal.

Fig. 5 shows the convergence of the proposed scheme in terms of the WASR versus the number of iterations in different scenarios. The results illustrate the convergence of the proposed scheme in terms of jointly optimized transmit power and trajectory for the aerial base station. One can observe that the WASR increases quickly within a small number of iterations and converges within around eight iterations in the listed three scenarios.

Fig. 6 shows the effect of the IT threshold on the WASR of different schemes. It can be observed that, as the threshold

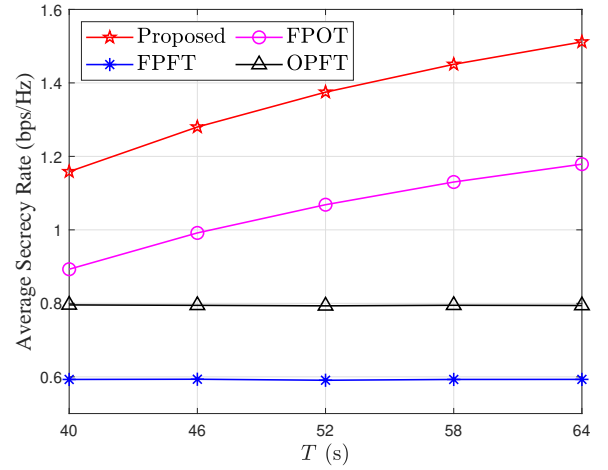


Fig. 7: The WASR of scenario 1 under different schemes versus T .

increases, the curves corresponding to the proposed and OPFT schemes show an increasing trend while those to FPFT and FPOT schemes remain constant. The reason is as Γ_r increases, the optimized transmit power increases, allowing the secrecy rate of the system to be improved. In the lower- Γ_r region, the transmit power of S is lower since the average interference power caused by S and eavesdroppers must be limited to the IT threshold to ensure that the QoS of the primary users is not affected. Thus, the secrecy rates with the proposed scheme and FPOT scheme outperform those with FPFT and OPFT schemes. Moreover, the curves for the proposed and OPFT schemes have the apparent increasing trend because Γ_r directly affects the transmit power of S since the transmit powers in the proposed and OPFT schemes are adaptively changed while the transmit power in FPFT and FPOT schemes are fixed. When the IT threshold reaches a certain value, the system becomes a non-cognitive mode where the transmit power is limited by the maximum transmit power of S . Then the WASR is independent of the IT threshold in the larger- Γ_r region.

Fig. 7 indicates the WASR versus the flight period T for the considered system under different schemes. It can be observed that the WASR of the considered system obtained by the proposed scheme outperforms those of others schemes. This is because both the UAV's trajectory and transmission power are jointly optimized in the proposed scheme simultaneously.

VI. CONCLUSION

This work investigated the security of aerial CRNs with multiple uncertainty FD eavesdroppers. By jointly designing the aerial base station's trajectory and transmission power, the WASR is formulated as a non-convex maximization problem. Based on BCD and SCA technologies, a new efficient iterative algorithm is proposed to solve the non-convex problem, and suboptimal solutions are obtained. Numerical results verified the convergence and effectiveness of our proposed algorithm. The A2G links in this work are assumed to be LoS links. In some scenarios, the A2G links are LoS links with elevation angle-dependent and environment-dependent probability. Thus, designing the 3D trajectory will be an interesting

problem in the future work. Considering the distribution of the eavesdroppers' location is also an interesting work and will be part of the future work.

REFERENCES

- [1] Y. Zeng, Q. Wu, and R. Zhang, "Accessing from the sky: A tutorial on UAV communications for 5G and beyond," *Proc. IEEE*, vol. 107, no. 12, pp. 2327-2375, Dec. 2019.
- [2] B. Li, Z. Fei, and Y. Zhang, "UAV communications for 5G and beyond: Recent advances and future trends," *IEEE Internet Things J.*, vol. 6, no. 2, pp. 1-23, Apr. 2019.
- [3] Q. Wu, L. Liu, and R. Zhang, "Fundamental trade-offs in communication and trajectory design for UAV-enabled wireless network," *IEEE Wireless Commun.*, vol. 26, no. 1, pp. 36-44, Feb. 2019.
- [4] C. Yan, L. Fu, J. Zhang, and J. Wang, "A comprehensive survey on UAV communication channel modeling," *IEEE Access*, vol. 7, pp. 107769-107792, Aug. 2019.
- [5] Q. Wu, Y. Zeng, and R. Zhang, "Joint trajectory and communication design for multi-UAV enabled wireless networks," *IEEE Trans. Wireless Commun.*, vol. 17, no. 3, pp. 2109-2121, Mar. 2018.
- [6] A. Bejaoui, K.-H. Park, and M.-S. Alouini, "A QoS-oriented trajectory optimization in swarming unmanned-aerial-vehicles communications," *IEEE Wireless Commun. Lett.*, vol. 9, no. 6, pp. 791-794, Jun. 2020.
- [7] J. Wang, C. Jiang, Z. Wei, C. Pan, H. Zhang, and Y. Ren, "Joint UAV hovering altitude and power control for space-air-ground IoT networks," *IEEE Internet Things J.*, vol. 6, no. 2, pp. 1741-1753, Apr. 2019.
- [8] L. Yang, H. Yao, J. Wang, C. Jiang, A. Benslimane, and Y. Liu, "Multi-UAV-enabled load-balance mobile-edge computing for IoT networks," *IEEE Internet Things J.*, vol. 7, no. 8, pp. 6898-6908, Aug. 2020.
- [9] T. Liu, M. Cui, G. Zhang, Q. Wu, X. Chu, and J. Zhang, "3D trajectory and transmit power optimization for UAV-enabled multi-link relaying systems," *IEEE Trans. Green Commun. Netw.*, vol. 5, no. 1, pp. 392-405, Mar. 2021.
- [10] J.-H. Lee, K.-H. Park, Y.-C. Ko, and M.-S. Alouini, "Throughput maximization of mixed FSO/RF UAV-aided mobile relaying with a buffer," *IEEE Trans. Wireless Commun.*, vol. 20, no. 1, pp. 683-694, Jan. 2021.
- [11] C. Wang, X. Chen, J. An, Z. Xiong, C. Xing, N. Zhao, and D. Niyato, "Covert communication assisted by UAV-IRS," *IEEE Trans. Commun.*, vol. 71, no. 1, pp. 357-369, 2022.
- [12] C. Zhan, Y. Zeng, and R. Zhang, "Energy-efficient data collection in UAV enabled wireless sensor network," *IEEE Wireless Commun. Lett.*, vol. 7, no. 3, pp. 328-331, Jun. 2018.
- [13] W. Lu, P. Si, F. Lu, B. Li, Z. Liu, S. Hu, and Y. Gong, "Resource and trajectory optimization in UAV-powered wireless communication system," *Sci. China Inf. Sci.*, vol. 64, no. 4, pp. 1-14, Mar. 2021.
- [14] W. Luo, Y. Shen, B. Yang, S. Wang, and X. Guan, "Joint 3-D trajectory and resource optimization in multi-UAV-enabled IoT networks with wireless power transfer," *IEEE Internet Things J.*, vol. 8, no. 10, pp. 7833-7848, May. 2021.
- [15] Q. Wu, W. Mei, and R. Zhang, "Safeguarding wireless network with UAVs: A physical layer security perspective," *IEEE Wireless Commun.*, vol. 26, no. 5, pp. 12-18, Oct. 2019.
- [16] H.-M. Wang, X. Zhang, and J.-C. Jiang, "UAV-involved wireless physical-layer secure communications: Overview and research directions," *IEEE Wireless Commun.*, vol. 26, no. 5, pp. 32-39, Oct. 2019.
- [17] Z. Ullah, F. Al-Turjman, and L. Mostarda, "Cognition in UAV-aided 5G and beyond communications: A survey," *IEEE Trans. Cogn. Commun. Netw.*, vol. 6, no. 3, pp. 872-891, Sept. 2020.
- [18] G. Zhang, Q. Wu, M. Cui, and R. Zhang, "Securing UAV communications via joint trajectory and power control," *IEEE Trans. Wireless Commun.*, vol. 18, no. 2, pp. 1376-1389, Feb. 2019.
- [19] Y. Wang, L. Chen, Y. Zhou, X. Liu, F. Zhou, and N. Al-Dhahir, "Resource allocation and trajectory design in UAV-assisted jamming wideband cognitive radio networks," *IEEE Trans. Cogn. Commun. Netw.*, vol. 7, no. 2, pp. 635-647, Jun. 2021.
- [20] B. Duo, J. Luo, Y. Li, H. Hu, and Z. Wang, "Joint trajectory and power optimization for securing UAV communications against active eavesdropping," *China Commun.*, vol. 18, no. 1, pp. 88-99, Jan. 2021.
- [21] M. Cui, G. Zhang, Q. Wu, and D. W. K. Ng, "Robust trajectory and transmit power design for secure UAV communications," *IEEE Trans. Veh. Technol.*, vol. 67, no. 9, pp. 9042-9046, Sept. 2018.
- [22] C. Zhong, J. Yao, and J. Xu, "Secure UAV communication with cooperative jamming and trajectory control," *IEEE Commun. Lett.*, vol. 23, no. 2, pp. 286-289, Feb. 2019.
- [23] R. Zhang, X. Pang, W. Lu, N. Zhao, Y. Chen, and D. Niyato, "Dual-UAV enabled secure data collection with propulsion limitation," *IEEE Trans. Wireless Commun.*, vol. 20, no. 11, pp. 7445-7459, Jun. 2021.
- [24] W. Wang, X. Li, R. Wang, K. Cumanan, W. Feng, Z. Ding, and O. A. Dobre, "Robust 3D-Trajectory and time switching optimization for dual-UAV-enabled secure communications," *IEEE J. Sel. Areas Commun.*, vol. 39, no. 11, pp. 3334-3347, Nov. 2021.
- [25] Y. Zhou, F. Zhou, H. Zhou, D. W. K. Ng, and R. Q. Hu, "Robust trajectory and transmit power optimization for secure UAV-enabled cognitive radio networks," *IEEE Trans. Commun.*, vol. 68, no. 7, pp. 4022-4034, Jul. 2020.
- [26] P. X. Nguyen, V.-D. Nguyen, H. V. Nguyen, and O.-S. Shin, "UAV-assisted secure communications in terrestrial cognitive radio networks: Joint power control and 3D trajectory optimization," *IEEE Trans. Veh. Technol.*, vol. 70, no. 4, pp. 3298-3313, Apr. 2021.
- [27] S. Liu, Y. Yu, L. Guo, P. L. Yeoh, B. Vucetic, Y. Li, and T. Q. Duong, "Satisfaction-maximized secure computation offloading in multi-eavesdropper MEC networks," *IEEE Trans. Wireless Commun.*, vol. 21, no. 6, pp. 4227-4241, Jun. 2022.
- [28] H. Lei, H. Yang, K. H. Park, I. S. Ansari, J. Jiang, and M. S. Alouini, "Joint trajectory design and user scheduling for secure aerial underlay IoT systems," *IEEE Internet Things J.*, vol. 10, no. 15, pp. 13637-13648, Aug. 2023.
- [29] J. Yao and J. Xu, "Joint 3D maneuver and power adaptation for secure UAV communication With CoMP reception," *IEEE Trans. Wireless Commun.*, vol. 19, no. 10, pp. 6992-7006, Oct. 2020.
- [30] Y. Gao, H. Tang, B. Li, and X. Yuan, "Energy minimization for robust secure transmission in UAV networks with multiple colluding eavesdroppers," *IEEE Commun. Lett.*, vol. 25, no. 7, pp. 2353-2357, Jul. 2021.
- [31] H. Fu, Z. Sheng, A. A. Nasir, A. H. Muqaibel, and L. Hanzo, "Securing the UAV-aided non-orthogonal downlink in the face of colluding eavesdroppers," *IEEE Trans. Veh. Technol.*, vol. 71, no. 6, pp. 6837-6842, Jun. 2022.
- [32] B. Liu, Y. Wan, F. Zhou, Q. Wu, and R. Q. Hu, "Resource allocation and trajectory design for MISO UAV-assisted MEC networks," *IEEE Trans. Veh. Technol.*, vol. 71, no. 5, pp. 4933-4948, May 2022.
- [33] M. Hua, L. Yang, Q. Wu, and A. L. Swindlehurst, "3D UAV trajectory and communication design for simultaneous uplink and downlink transmission," *IEEE Trans. Veh. Technol.*, vol. 68, no. 9, pp. 5908-5923, Sept. 2020.
- [34] S. Boyd and L. Vandenberghe, *Convex Optimization*: Cambridge Univ Press, 2004.